Volume 119 | Issue 1 | January 5, 2019

# International Journal of QUANTUM CHEMISTRY

www.q-chem.org

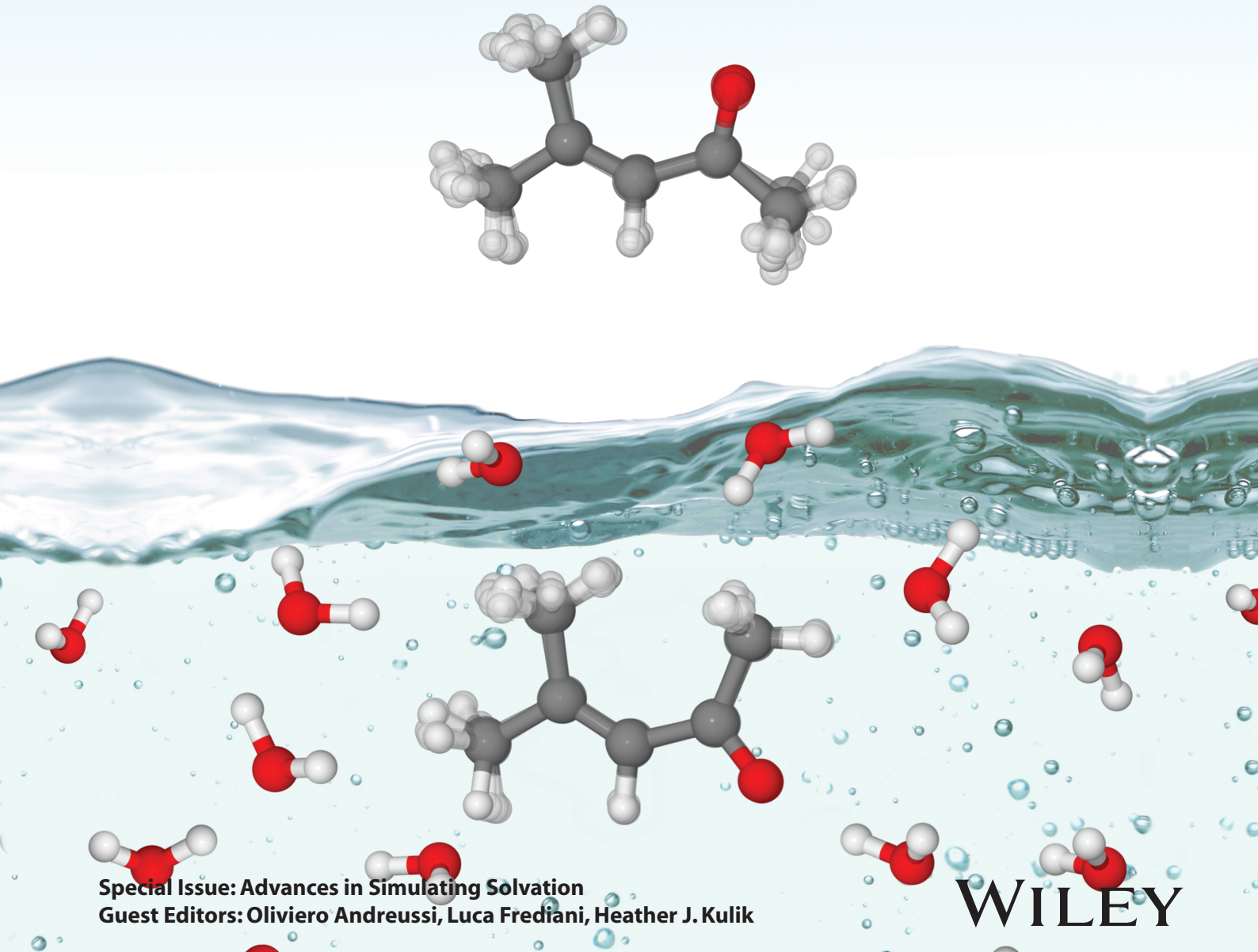

Special Issue: Advances in Simulating Solvation
Guest Editors: Oliviero Andreussi, Luca Frediani, Heather J. Kulik

WILEY

Received: 18 April 2018 | Accepted: 21 May 2018

DOI: 10.1002/qua.25688

WILEY International Journal of QUANTUM CHEMISTRY

FULL PAPER

# Solvent effect on the *syn/anti* conformational stability: A comparison between conformational bias Monte Carlo and molecular dynamics methods

**Henrique M. Cezar | Sylvio Canuto | Kaline Coutinho**

Departamento de Física Geral, Instituto de Física, Universidade de São Paulo, São Paulo, Brazil

**Correspondence**
Kaline Coutinho, Instituto de Física, Universidade de São Paulo, São Paulo, Brazil.
Email: kaline@if.usp.br

**Funding information**
Fundação de Amparo à Pesquisa do Estado de São Paulo; Conselho Nacional de Desenvolvimento Científico e Tecnológico; Coordenação de Aperfeiçoamento de Pessoal de Nível Superior

The solvent effect on the *syn/anti* population ratio of the mesityl oxide (MOx) was investigated using a new implementation of conformational bias Monte Carlo (CBMC) and molecular dynamics (MD) methods. It was observed by a previous theoretical work (Theor. Chem. Acc. (2012) 131:1214) that in gas-phase the MOx exists dominantly in *syn*-form and in aqueous solution in *anti*-form. The *syn/anti* free energy difference in the gas phase was used in the intramolecular parametrization and a rotational barrier of approximately 10 kcal $mol^{-1}$ was found. Molecular systems with barriers of this order of magnitude have been studied by experimental techniques. However, they have not been discussed yet comparing CBMC and MD simulations. In this work, we show that the intramolecular geometrical information such as bond lengths, angles and torsional angles sampled with CBMC and MD methods are equivalent. Nonetheless, only the CBMC simulations sample appropriately the *syn/anti* population ratio. With the CBMC configurations in gas phase, it was obtained 95% in *syn*-form and 5% in *anti*-form regardless the initial conformation. An inversion of the population was found in water, 25% in *syn*-form and 75% in *anti*-form. Comparing the gas phase and in-water CBMC sampling, it was observed that the MOx spends typically approximately 110 successive MC cycles in *anti*-form and approximately 2300 in *syn*-form in gas phase. While it was much larger with explicit water, approximately 400 times more for *anti*-form and approximately 6 times more for *syn*-form. We argue that this strong stabilization of the *anti*-form in aqueous solution, does not come from the MOx-water hydrogen bonds interactions, because they are the same for both conformations. Instead, the stabilization comes from the dipole-dipole interaction caused by a larger dipole moment of the MOx in the *anti*-form, 7.2 D, than in the *syn*-form, 5.2 D. With the MD sampled configurations in both conditions, we observe that the *syn/anti* conformational change is a very rare event due to the rotational barrier, which is approximately 17 times larger than the thermal energy. Therefore, the MD sampling of the MOx is not appropriated because it is strongly dependent on the initial conformation even for large simulations with 150 ns up to 400 ns for the isolated solute and for solute–solvent systems. 

**KEYWORDS**

configurational bias Monte Carlo, MC versus MD, solvent effects, syn/anti stability

## 1 | INTRODUCTION

The properties of a molecule are closely related to its geometry. It is well known that the solvent can provide changes in the conformational stability of solvated molecules changing either the relative free energy of different conformers or the height of the barriers, that is, activation enthalpy that will change the kinetic process. Thus, the study of solvent effects on conformational stability is an important topic and has been studied by experimental and theoretical techniques.[1,2] It can be found in the literature examples of experimental studies with infrared (IR) spectroscopy

where the environment is able to change the conformational population ratio. This is the case of 1,2-dichloro, 1,2-dibromo, and 1-chloro-2-bromoethane that present conformational *trans/gauche* population ratio of 77%, 90%, and 83% in vapor phase and 35%, 64%, and 54% in liquid phase, respectively.[3] Additionally, another study[4] for 1,2-dichloroethane presented the following values of the *trans/gauche* population ratio 79% in gas phase, 62% in cyclohexane, 54% in di-n-butyl ether, 38% in tetrahydrofuran, 28% in acetone, and 26% in acetonitrile and for 1-chloro-2-fluoroethane they are 56%, 37%, 27%, 16%, and 10%, respectively. Another powerful technique to measure the equilibrium population ratio of conformers and also identify its conformational barrier in solution is the nuclear magnetic resonance (NMR) spectroscopy.[5–9]

From the theoretical point of view, there are many studies of conformational stability using ab initio calculations with quantum mechanics (QM) in vacuum and in solution with the solvent effect described by the polarizable continuum model (PCM) or solvent-clusters.[7,9–12] However, another well-known approach to describe the solvent and its interactions with solute molecules is using computer simulations with Monte Carlo (MC) or molecular dynamics (MD) methods.[13,14] The ergodic hypothesis states that these two methods are equivalent when the simulations are infinitely long, because both methods can sample all the configurational space. But for finite simulations one method can be better than the other, due to the difference in the procedure to generate the solute–solvent configurations. The MC method is based on the probabilistic Metropolis sampling technique to generate the configurations. Therefore, the ergodicity of the MC simulations is guaranteed by the detailed balance condition independently of the size of the conformational barriers. Conversely, the MD method is based on the solution of the Newton equations of motion. Then, the solute–solvent conformations will be generated following the potential energy surface and the conformational barriers will play an important role in the ergodicity of the simulation, because large barriers impose large time length (seconds or hours) that cannot be reached by finite MD simulations. Thus, it is known that for sampling conformations with large barriers the MD method is not recommended and other techniques should be coupled to the MD method to enhance the conformational sampling, such as temperature replica exchange molecular dynamics methods,[15] biased molecular dynamics method,[16] and several others.[17]

There are some works in the literature[18,19] that compared the conformational sample with MC and MD simulations for small systems with low conformational barriers (around 3-4 kcal/mol). The main conclusions are that both methods successfully sample the conformational space. Additionally, independent studies performed with MC simulation[20,21] and ab initio MD simulation[22] showed the same sampling of a solute conformational change from low polarity solvent to aqueous solution. In these studies, the solute changes from the conformation with approximately 30° of the torsional angle between two specific rings of the solute in low polarity solvent (or gas phase) to approximately 60° in aqueous solution. For this system no rotational barrier was identified due to a very complex rotational process driven by an intramolecular charge transfer in solution that gives a free energy difference of approximately 3.5 kcal/mol.[21] Therefore, this example emphasizes again the good agreement between the MC and MD conformational sampling.

Although the cases discussed above with small energy barriers have been well studied, the cases of large barriers (around or larger than 10 kcal/mol) have not been discussed yet comparing MC and MD simulations. Therefore, this investigation is timely and important. For these kind of systems there are experimental measurements with NMR spectroscopy for different types of conformational equilibrium, such as axial/equatorial population ratio of 50% with a rotational barrier of approximately 10 kcal/mol,[5] *syn/anti* population ratio of 95% with a rotational barrier of approximately 11 kcal/mol,[6] and *cis/trans* population ratio of 85% with an activation barrier of approximately17 kcal/mol.[8]

In this work, we studied the solvent effect on the *syn/anti* conformational stability using a new implementation of the Configurations Bias Monte Carlo (CBMC) method for sampling the internal flexibility of a solute molecule in gas phase and in aqueous solution. In the CBMC method a new conformation of a selected molecule is generated following one of the several approaches developed throughout the years.[23–28] The movements of the atoms inside the molecules are divided in two types: the hard degree of freedom, in general are the bonds and angles vibrations, and the soft degrees of freedom that are the rotational movements of torsional angles. This separation of hard and soft degrees of freedom is necessary, because they have energies that are different by orders of magnitude, where the energy changes involved in the hard movements are much larger than the soft movements. However, the conformational changes are dominated by the soft degrees of freedom rather than the hard ones. For this reason, the biased movement in the CBMC methods is applied in the soft degrees of freedom, aiming a more efficient generation of new conformations.

In our implementation of the CBMC method, the molecule is previously divided in fragments, composed by the hard degrees of freedom. Since the relative motion between the successive fragments is a rotation, then each fragment must have in common two atoms forming a chemical bond that belongs to both fragments. These fragments are put together around this common bond with different biased selected torsional angles in each simulation step. The procedure implemented by us to generate a new conformation of a random selected molecule in the CBMC simulation is: (i) select by random one fragment and one side to be rebuild, (ii) delete all fragments of this selected side, (iii) select a configuration for each fragment from a previously sampled fragment library of deformations, (iv) generate new torsional angles following the Boltzmann probability defined among a finite set of trial insertion angles for rebuild all fragments until the deleted side is fully regrown. The new conformation will be accepted or rejected based on an acceptance criterion, which takes into account the interactions of the molecule itself and with the solvent around in the new and old conformations. This CBMC approach of splitting the molecule into fragments and rebuilding joining these fragments to generate new conformational states was developed by Macedonia and Maginn[28] and later extended by Shah and Maginn.[25] The procedure of sampling the inner fragment deformations follows already proposed methods[25] and also new approaches presented in this work. Additionally, we made simplifications in the analytical expression of the acceptance criterion and solve numerical instabilities in the algorithm.

We choose the mesityl oxide (MOx) molecule [$(CH_3)_2C{=}CHC(=O)CH_3$, 4-methyl-3-penten-2-one] to investigate the solvent effect on the conformational stability using CBMC and MD simulations in gas phase and in aqueous solution. The MOx is a model for larger species of ketones

characterized by the carbonyl group (–C=O) linked with two other organic groups, R1CH–C(=O)–[CR2. Therefore, the rotation around the single bond between the R1CH– and the –C(=O)–CR2 can generate a *syn* or *anti* conformations (see Figure 1 for the MOx case). When this C=C–C=O dihedral angle is 0° the MOx is in the *syn*-form while an angle of 180° is the *anti*-form. Based on the IR and UV-visible spectroscopy[29–31] it was identified that the *syn/anti* population ratio of the MOx is solvent dependent, but it was not possible to measure experimentally due to the coexistence of the MOx and the iso-mesityl oxide (IMOx) molecule [$CH_3$–C(=$CH_2$)$CH_2$C(=O)$CH_3$, 4-methyl-4-penten-2-one] in the system. However, the MOx was only studied in gas phase and in aqueous solution with theoretical methods[32] using QM calculations and MC simulations with rigid model of the MOx in the *syn*- and *anti*-forms. The free energy differences between the *syn*- and *anti*-forms were calculated and also the shift of $\pi-\pi^*$ excitation energy due to the conformational change and the solvent polarity. The theoretical results are in good agreement with the experimental measurements. Thus, the main conclusion is that the MOx has lager population in the *syn*-form in gas phase or in solvent with low polarity and larger population in the *anti*-form in aqueous solution. Therefore, the MOx is a small molecule that presents solvent dependent *syn/anti* population ratio and is a model for a large class of non-saturated $\alpha$-$\beta$-ketone molecules. Additionally, it presents a large rotational barrier (~10 kcal/mol) that will be discussed in a later section of this work.

## 2 | THEORETICAL DETAILS

We implemented the CBMC method in the software DICE.[33,34] The first work published using this software was in 1993 for liquid benzene MC simulations,[35] and since then it has been continuously updated. However, the name DICE was first cited in only in 1997.[36] This software performs MC simulations of rigid molecules in the NVT or NPT ensembles with the molecular interaction described by the Lennard–Jones and Coulomb potentials. It uses standard procedures,[13,14] such as random selection of one molecule for each MC step, translational displacements in Cartesian coordinates with an auto-adjusted maximum value, rotational movements around a random axis, isotropic volume re-scale (in the NPT ensemble), Metropolis sampling technique, periodic boundary condition, image method, neighbor list, cutoff radius implementation, and calculation of the long range correction of the energy with the self-consistent reaction field (SCRF) approximation. Additionally, there are some non-standard procedures: (i) hard sphere potential, (ii) preferential sampling with the one-over-$r^n$ algorithm,[37,38] and (iii) calculations of free energy differences using the free energy perturbation (FEP).[39,40]

### 2.1 | Configurational bias Monte Carlo

The main goal of the CBMC method is to build a molecule piece by piece in a way that the intra and intermolecular energies are sampled appropriately and efficiently. The general procedure generates a new molecular conformation using a series of subsequential growth steps. In each growth step, there is an attempt to find new and reasonable positions for a piece of the molecule that is defined with a small set of atoms. There are several different procedures for the CBMC method in the literature.[23–28] They differ in many small details that are used to define the pieces of the molecule, to select the pieced and to attempt to change their positions in a given growth step. We use the CBMC procedure developed by Shah and Maginn[25] to define pieces of the molecule (fragments), to select the successive fragments to be deleted and rebuild in subsequential growth steps until a new conformation of the molecule is generated. In the Shah and Maginn CBMC approach,[25] the molecule is initially divided in $N_{frag}$ fragments. The fragments are composed by the hard degrees of freedom (represented by $\{\theta\}$), that is, the degrees of freedom that will fluctuate around an equilibrium value, such as bending angle and improper dihedrals. Therefore, it can be noticed that these inner fragment deformations do not generate substantial changes in the molecular conformation. A library of possible inner deformations of each fragment is generated before the growth steps. These deformations are based on branch point sampling for simple fragments or crankshaft movements for simple rings. Then, a new conformation of the whole molecule is generated after selecting one fragment randomly and one of its side to be deleted and rebuild using the growth steps to rebuild this deleted part of the molecule. Therefore, only one part of the molecule will attempt to be rebuild in each CBMC step. The growth steps, that compose one CBMC step, make the reinsertion of new deformed fragments, selected from the library, with new

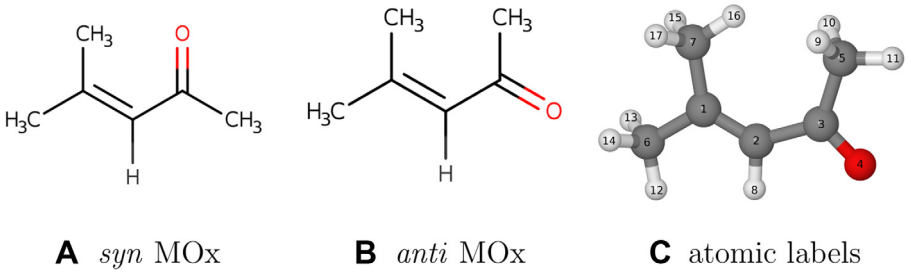


**FIGURE 1** Mesytil oxide (MOx) in the (A) *syn* and (B) *anti* configurations. The (C) figure shows the atomic labels in a 3D representation of the *anti* conformation. The C=C–C=O torsion referred in the text is the resulting sum of four dihedral angle contributions defined by the atoms 1-2-3-4, 1-2-3-5, 8-2-3-4, and 8-2-3-5

dihedral angles in the connections. These dihedral angles that join successive fragments are the soft degrees of freedom (represented by $\{\phi\}$). Several possible insertion dihedral angles are generated for each fragment insertion, and based on those trials the acceptance probability is calculated.

## 2.2 | New ideas on the CBMC implementation

In our implementation of the CBMC method, we further simplify the acceptance criterion for the canonical ensemble,[25] leaving the expression less prone to numerical errors. This simplification is achieved by noticing that the forward and reverse moves in the detailed balance have the same energy for the fragments that were not rebuild. The total energy $U = U(\{\theta\}) + U(\{\phi\})$ can be written as a sum of the energies of the hard, $U(\{\theta\}) = \sum_{i=1}^{N_{\text{frag}}} u(\{\theta_i\})$, and soft, $U(\{\phi\}) = \sum_{i=1}^{N_{\text{frag}}} u(\{\phi_i\})$, degrees of freedom, where $N_{\text{frag}}$ is the number of fragments of the molecule. If only $N_{\text{del}}$ fragments are rebuilt in each CBMC step, the energy of these fragments can be further separated by the other terms in the sum. The fragments that were kept rigid during this CBMC step, $N_{\text{rig}} = N_{\text{frag}} - N_{\text{del}}$, will have the same energies in the forward and reverse moves, so only the $N_{\text{del}}$ rebuild fragments actually contribute to the acceptance probability. We define the Rosenbluth factor of the old $o$ configuration in the detailed balance as

$$W(o) = \prod_{i=1}^{N_{\text{del}}} \sum_{k=1}^{\kappa_\phi} \exp\left(-\beta u(\{\phi_{ik}^o\})\right), \tag{1}$$

where $\beta = (kT)^{-1}$ is the inverse of the thermal energy, $\kappa_\phi$ represents the number of trial insertion angles used in the CBMC move during the insertion of the fragments. This definition follows the usual definition of the Rosenbluth factors previously adopted in the CBMC,[14,23] and allows the acceptance criterion to be written just as

$$\text{acc}(o \to n) = \min\left(1, \frac{W(n)}{W(o)}\right), \tag{2}$$

where $o$ represent the old conformation and $n$ the new one.

Equation 2 is an improvement over the acceptance criterion proposed by Shah et al.,[41] however, due to the characteristic of the Rosenbluth factor that is a product of sums, the numerical instabilities are still a factor to be considered. Then, to minimize this problem, the acceptance criterion of Equation 2 was written as an exponential of a logarithm, ending with a difference of the log of the Rosenbluth factors in the new and old conformations:

$$\text{acc}(o \to n) = \exp[\min\left(0, \ln W(n) - \ln W(o)\right)], \tag{3}$$

where

$$\ln W(n) = \sum_{i=1}^{N_{\text{del}}} \ln[\sum_{k=1}^{\kappa_\phi} \exp\left(-\beta u(\{\phi_{ik}^n\})\right)]. \tag{4}$$

The sum of exponentials in Equation 4 can still lead to numerical problems, since the exponentials might result in large or small values that cannot be represented by a floating point in a given precision. This problem can be solved by taking the largest argument $x_1$ of the exponential out of the summation as follows

$$\ln \sum_{i=1}^{N} e^{x_n} = \ln\left(\sum_{i=1}^{N} e^{x_n} \frac{e^{x_1}}{e^{x_1}}\right) = x_1 + \ln\left(1 + \sum_{i=2}^{N} e^{x_n - x_1}\right), \tag{5}$$

so the differences $x_n - x_1$ are always smaller and closer to zero than the initial arguments themselves. For Equation 4, the largest argument $x_1$ corresponds to lowest energy obtained among the $\kappa_\phi$ trial insertion angles. Then, applying this concept to the log of the Rosenbluth factor, presented in Equation 1, we finally have the acceptance criterion given by Equation 3 with the log of the Rosenbluth factor written as

$$\ln W(n) = \sum_{i=1}^{N_{\text{del}}} -\beta u(\{\phi_{i1}^n\}) + \ln\left\{1 + \sum_{k=2}^{\kappa_\phi} \exp\left[-\beta\left(u(\{\phi_{ik}^n\}) - u(\{\phi_{i1}^n\})\right)\right]\right\}. \tag{6}$$

Additionally, we propose a new method to generate the fragment libraries for general fragments. Since the only assumption about the fragment libraries is that the configurations were sampled from a Boltzmann distribution of states, it is possible to perform a MC simulation with Cartesian displacements and accepting with the Metropolis criterion to generate the fragment libraries. The advantage of this possibility is to introduce the bond length sampling that may not be relevant for the structural properties of the system, but can be important for electronic properties of the solute. This is the case of the C=O stretch that has effect in the electronic excitation of the acetone molecule in solution.[42] Although the Cartesian displacements are strictly correct, it is expected to be inefficient for large fragments but reasonable for small fragments. Therefore, the Cartesian displacements and completely rigid fragments were implemented as an alternative that can be used for any kind of fragment. For

fragments composed of simple branches and simple rings the previously proposed branch point sampling and crankshaft rotations algorithms[25] are still favored.

## 2.3 | Interatomic potential

We use the OPLS-AA force field to describe the interatomic interactions.[43] In this force field the bond, angle, and improper torsionals interactions are described as harmonic functions

$$u_{\text{bond}} = \sum_{\text{bonds}} K_r (r - r_{\text{eq}})^2, \tag{7}$$

$$u_{\text{angle}} = \sum_{\text{angles}} K_\theta (\theta - \theta_{\text{eq}})^2, \tag{8}$$

$$u_{\text{improper}} = \sum_{\text{improper}} K_\phi (\phi - \phi_{\text{eq}})^2, \tag{9}$$

and the torsional angles are described by Fourier terms

$$u_{\text{torsion}} = \sum_i \frac{V_1^i}{2}[1 + \cos(\phi_i + f_1^i)] + \frac{V_2^i}{2}[1 - \cos(2\phi_i + f_2^i)] + \frac{V_3^i}{2}[1 + \cos(3\phi_i + f_3^i)]. \tag{10}$$

Both intermolecular and intramolecular nonbonded interactions were described by the Lennard–Jones and Coulomb potentials

$$u_{\text{nb}} = \sum_i \sum_j f_{ij} \left\{ \frac{q_i q_j e^2}{r_{ij}} + 4\varepsilon_{ij} \left[ \left( \frac{\sigma_{ij}}{r_{ij}} \right)^{12} - \left( \frac{\sigma_{ij}}{r_{ij}} \right)^{6} \right] \right\}, \tag{11}$$

where $r_{ij}$ is the distance between the atoms $i$ and $j$, $q_i$ represents the charge, and $\varepsilon_i$ and $\sigma_i$ are the Lennard–Jones parameters for each interacting site $i$. The two usual combination rules for the Lennard–Jones parameters $\varepsilon_{ij} = (\varepsilon_i \varepsilon_j)^{1/2}$ and $\sigma_{ij} = (\sigma_i \sigma_j)^{1/2}$ or $\sigma_{ij} = (\sigma_i + \sigma_j)/2$ can be employed. As usual for OPLS-AA, the 1-4 intra-molecular interactions are scaled by $f_{ij} = 0.5$, while more further interactions $f_{ij} = 1.0$.

For the case of MOx, we used the parameters previously used.[32] All the nonbonded parameters of MOx, except the atomic charges, were taken from the OPLS-AA force field, and water was described by the SPC/E model.[44] The atomic charges were obtained before[32] considering implicit polarization of the aqueous solution[45] using the CHELPG procedure[46] to fit the electrostatic potential generated in the QM calculations at MP2/aug-cc-pVDZ level[47,48] for the *syn* and *anti* conformations. In this work, the atomic charges were calculated as an rounding of the average charges in both conformers. This new set of atomic charges cause a small difference in the dipole moment of the MOx in each conformation. The dipole moment calculated previously[32] were 4.97 D for the *syn* conformation and 6.96 D for the *anti* conformation and the values obtained here are 5.22 D and 7.20 D, respectively. The bonded parameters were also taken from OPLS-AA. However, the torsional angle responsible for the *syn*:*anti* conformation, defined by C=C–C=O (see Figure 1), was adjusted to have the value of the energy difference of the *syn*:*anti* conformations equal to the value previously calculated for the free energy difference of these conformations.[32] All the parameters that were used in our simulations are available in the Supporting Information.

## 2.4 | Simulation details

All the CBMC simulations were run in DICE,[49] using our implementation of the Shah and Maginn method[25] described in subsection configurational bias Monte Carlo and our new ideas in subsection new ideas on the CBMC implementation. The simulated system was composed by one MOx molecule and 1200 water molecules in the NPT ensemble with the number of molecules $N = 1201$, the pressure $P = 1$ atm and the temperature $T = 300$ K. Periodic boundary conditions were employed in a cubic box with the edge of initial length of $L = 33.04$ Å giving a density of 1 g/cm$^3$. The cutoff radius was $r_c = 0.8 \times L/2 \approx 15$ Å and the long range corrections were calculated beyond this cutoff.[13] To improve the sampling of the solute and its surroundings we have used a preferential sampling scheme with $n = 2$. We also performed a NVT simulation for the gas phase to check if the *syn*/*anti* population reflected the populations expected by the potential. In the gas phase simulation only one MOx molecule was placed in the box, in the same temperature of the simulations in aqueous solution.

The MOx molecule was broken in five fragments for the CBMC simulation. Those fragments can be seen in Figure 2, where each fragment is also labeled with a number. As it can be seen, the fragments 3, 4, and 5 are the most simple and responsible for the rotation of $CH_3$ groups in the MOx molecule. These fragments were sampled with the branch point sampling algorithm, where the atoms are displaced in spherical coordinates with rigid bonds and flexible angles to create the libraries of each fragment. The fragment 2 was sampled with Cartesian displacements, because we would like to sample the C=O bond stretch and the –C–C=O angle. The fragment 1 could be split in two branch fragments; however, since the bond between these two fragments is the C1 C2 double bond, it would lower the CBMC acceptance rates as the potential for rotations around this bond is very stiff. For this reason we defined the fragment 1 as a single fragment and, like the fragment 2, it was sampled with Cartesian displacements. The library of each fragment was composed of 10 000 independent conformations previously sampled from the gas phase simulations of the isolated fragment performed with $2 \times 10^8$ MC steps and stored in the last half of the simulation.

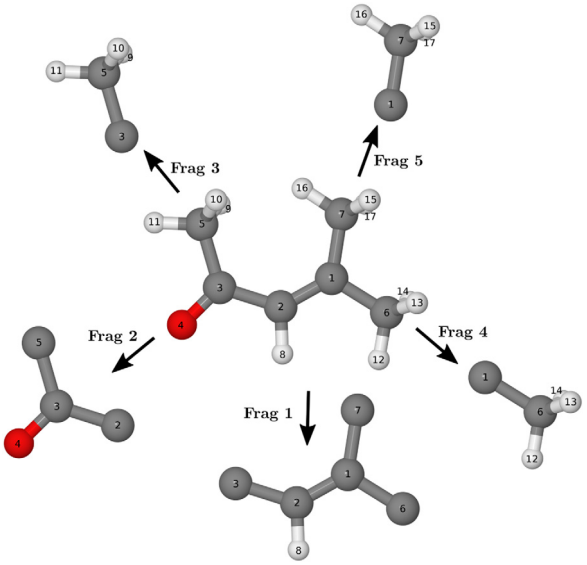


**FIGURE 2** Fragmentation scheme used for the CBMC simulation of MOx molecules

We have used $\kappa_\phi = 32$ trial insertion angles for trying to rebuild each fragment in a CBMC step and generating a new conformation. These trial angles were generated with the value of the first angle randomly selected and the remaining ones evenly distributed in the $2\pi$ interval. The energies of these trial angles were used to Equation 6 to calculate the $\ln W(n)$ that will be needed to calculate the acceptance criterion (see Equation 3). To calculate the ln $W(o)$ a reverse regrowth process is necessary, that is, generating the old conformation starting from the new one. Therefore, in this reverse process, one of the 32 trial angles that will be selected should be the dihedral angle of the old conformation. Then, to ensure this compulsory selection one angle of the trial set is the dihedral angle of the old conformation and the others 31 remaining angles were generated using the same procedure of the forward rebuild process.

In the gas phase simulation, every move was a CBMC step trying to rebuild the molecule from a random fragment, while for the water simulation, when the MOx molecule was selected it had 80% of chance to be rebuild with the CBMC scheme and 20% to be translated and rotated around a random axis. A total of $10^6$ MC steps were performed for the MOx in gas phase simulation. The CBMC simulation of MOx in aqueous solution was started from an already thermalized box with the MOx molecule in either the *syn* or *anti* configurations. To thermalize the system $3 \times 10^8$ MC steps were performed. After that, the CBMC simulations were performed for $48 \times 10^8$ MC steps. Of those CBMC simulation steps in water, only the last MC steps were considered to calculate the percentage of *syn:anti* conformers. For a better comparison of the MC steps with the MD integration step, instead of using the unit of a MC step, we define a MC cycle, which is composed by $N$ MC steps. Therefore, in one MD step and in one MC cycle, the $N$ molecules of the system were moved or at least there was the attempt to move.

The MD simulations were performed using GROMACS version 5.1.4.[50] We used the same quantity of molecules, the same ensemble (isothermal-isobaric) and thermodynamic conditions as described above for the CBMC simulations. The temperature was kept at 300 K by the velocity rescale thermostat,[51] using a coupling constant of 0.1 ps. Pressure was maintained constant at 1 atm by an isotropic Berendsen barostat[52] with a compressibility of $4.5 \times 10^{-5}$ and coupling constant of 0.1 ps. The equations of motion were integrated with the leap-frog algorithm and a time step of 2 fs. All the H bond lengths were constrained using the LINCS algorithm.[53]

For the gas phase, the MD simulations were performed during 400 ns for each initial conformation. For the MOx simulation in water the two trajectories, starting from the *syn* and *anti* conformations, were also integrated for 400 ns. Two other water simulations were performed with 150 ns each, to check when the conformational changes started.

## 3 | RESULTS

### 3.1 | Mesityloxide parametrization

Using the set of nonbonded parameter $\{q_i, \varepsilon_i, \sigma_i\}$ of the previous work[32] and the bonded parameters chosen from the OPLS-AA force field for ketones, we obtained an energy profile around the C=C–C=O torsional angle that present minima at around ±180°, ± 120°, and ± 60°. These minima indicate that the *gauche*, *eclipsed*, and *anti* conformations are the most stable conformations (in this order) and the *syn* conformation is an instable one. But these minima are not in agreement with the ab initio energies previously calculated.[32] In this calculations performed at MP2/aug-cc-pVDZ level in gas phase, the stable conformations were the *syn*- and *anti*-forms with a free energy difference of 1.34 kcal/mol in favor of the *syn* conformation. Then, to have a classical intramolecular potential in agreement with this ab initio free energy difference, we re-parameterized the four dihedral angles that defines the rotation on the C=C–C=O group (see Figure 1). The new values obtained by us for $V_1^i$, $V_2^i$,

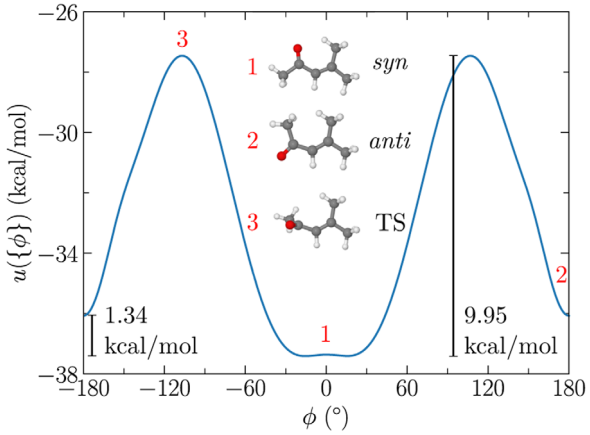


**FIGURE 3** Energy profile of the rotation in the C–C–C–O group that defines the *syn:anti* conformers. During the rotation both parts of the molecule were kept rigid

and $V_3^i$ (see Equation 10) were: −1.8 kcal/mol, 4.3 kcal/mol, and −1.9 kcal/mol for the dihedral angle 1-2-3-4; 1.4 kcal/mol, 5.2 kcal/mol, and −4.7 kcal/mol for the dihedral angle 1-2-3-5; 0.0 kcal/mol, 0.0 kcal/mol, and 0.7/kcal mol for the dihedral angle 8-2-3-5; and 0.0 kcal/mol for the dihedral angle 8-2-3-4. All the $f_1^i$, $f_2^i$, and $f_3^i$ were zero.

In Figure 3 the re-parameterized energy profile of the internal rotation in the C=C–C=O group is shown. In this total potential energy calculations all bonded and nonbonded parameters of the intramolecular force field were considered keeping rigid all other degree of freedom during the rotation. The rotational barrier obtained between the *syn* conformation and the transition state (TS) is 9.95 kcal/mol. Although this value of the rotational barrier is very high, it was the lowest value that we could obtained using the nonbonded parameters defined before[32] to study the solvent effect on the *syn:anti* relative population. Since we are mostly interested in the equilibrium population of the conformers and differences between the sampling of CBMC and MD, the most important feature of the potential energy surface is the relative stability between the two relevant conformers. The high rotational barrier only poses as an extra challenge for the sampling.

## 3.2 | Comparison of the CBMC and MD sampling

We use the MD sampling of the internal degrees of freedom of the MOx in gas phase and in aqueous solution as a validation test of our implementation of the CBMC method. In Table 1 we present the average values and standard deviations of some important geometrical information such as bond lengths, angles, and torsional angles sampled in the CBMC and MD simulations. As it can be seen, the average values sampled with the CBMC are all in agreement

**TABLE 1** Geometric information of the MOx obtained in the CBMC and MD simulations in both gas phase and in water

| | Gas phase | | In aqueous solution | |
|---|---|---|---|---|
| | CBMC | MD | CBMC | MD |
| $r_{C1C2}$ | 1.356 ± 0.016 | 1.360 ± 0.024 | 1.356 ± 0.016 | 1.359 ± 0.023 |
| $r_{C2C3}$ | 1.486 ± 0.019 | 1.488 ± 0.028 | 1.486 ± 0.012 | 1.485 ± 0.027 |
| $r_{C3O4}$ | 1.227 ± 0.016 | 1.225 ± 0.024 | 1.235 ± 0.016 | 1.237 ± 0.023 |
| $\theta_{C1C2C3}$ | 133.9 ± 2.0 | 134.7 ± 2.8 | 134.8 ± 2.0 | 135.7 ± 2.8 |
| $\theta_{C2C3O4}$ | 117.7 ± 2.0 | 117.6 ± 2.8 | 116.7 ± 2.0 | 117.2 ± 2.9 |
| $\theta_{C6C1C7}$ | 112.5 ± 2.1 | 112.2 ± 2.8 | 112.4 ± 2.0 | 112.0 ± 2.8 |
| $\theta_{C6C1C7}$ | 112.5 ± 3.3 | 112.7 ± 4.7 | 112.6 ± 3.3 | 112.8 ± 4.6 |
| $\phi_{C6C1C2C3}$ | 180.0 ± 4.0 | 180.0 ± 5.9 | 180.0 ± 4.1 | 180.0 ± 5.8 |
| $\phi_{C1C2C3O4}$ | | | | |
| *syn* | 0.3 ± 19.8 | 0.0 ± 19.0 | 0.2 ± 25.3 | 0.0 ± 23.1 |
| | (0.1 ± 19.9) | (0.1 ± 19.9) | (2.0 ± 25.4) | (*) |
| *anti* | 179.8 ± 9.5 | * | 179.7 ± 10.1 | 180.0 ± 11.6 |
| | (179.7 ± 9.7) | (179.7 ± 9.7) | (179.7 ± 10.2) | (180 ± 11.5) |
| *syn:anti* ratio | 95:5 ± 1 | 100:0* | 22:78 ± 7 | 35:65 |
| | (96:4 ± 1) | (44:56) | (27:73 ± 10) | (0:100*) |

Distances *r* are shown in Å and angles in °. The values in parenthesis indicate data from simulations started in the *anti* conformation, all the other data is from simulations started in the *syn* conformation. The $\phi_{C1C2C3O4}$ line is splitted into *syn* and *anti* as the sampled distribution is bimodal. * indicates that only one conformation was sampled.

with the values sampled with MD and with the equilibrium values of the harmonic bonded potentials of the force field (described in Equations 7 and 8). These values are: $r_{eq(C1C2)} = 1.3535Å, r_{eq(C2C3)} = 1.4857Å, r_{eq(C3O4)} = 1.2291Å, \theta_{eq(C1C2C3)} = 133.09^{\circ}, \theta_{eq(C2C3O4)} = 117.48^{\circ}, \theta_{eq(C6C1C7)} = 113.12^{\circ}$, and $\theta_{eq(H12C6C1)} = 112.23^{\circ}$.

One particularly interesting angle to look at is the $\phi_{C6C1C2C3}$ dihedral. The final distribution of this dihedral angle was obtained with the rotation energy profile described by the sum of all the nonbonded potential terms and the four bonded torsional angles defined by the atoms: 6-1-2-3, 6-1-2-8, 7-1-2-3, and 6-1-2-8 (see Figure S1 in the Supporting Information). This energy profile has two minima, one at 180° corresponding to the *trans* conformation and other at 0° corresponding to the *cis* conformation. The most stable is the *trans* conformation by approximately 15 kcal/mol and with a rotational barrier of approximately 53 kcal/mol. Therefore, with this energy difference between the *cis*- and *trans*-forms, it is expected a pure population of the *trans*-form.

In our CBMC simulations, the $\phi_{C6C1C2C3}$ dihedral angle was sampled only during the generation of the fragment 1 library with Cartesian displacements and the Metropolis MC algorithm, because we defined all atoms of this dihedral belonging to the same fragment (see Frag 1 in Figure 2). As this fragment is fairly rigid and composed of few atoms, the Cartesian displacement sampling is good enough to generate a distribution of dihedral angles around the average value, $\langle \phi_{C6C1C2C3} \rangle = 180.0 \pm 4.0^{\circ}$, with similar standard deviation to the MD distribution, $180.0 \pm 5.9^{\circ}$. Therefore, we conclude that the Cartesian displacement sampling, as used to sample the translational and rotational degrees of freedom of the whole molecule, is a good choice of sampling procedure for this kind of fragment.

The Cartesian displacement sampling was also used in fragment 2 (see Frag 2 in Figure 2) and this allowed the analyzes of the C=O stretch due to hydrogen bonding. The branch point sampling keeps the bond lengths rigid, therefore, the use of this method to generate the fragment library is not an option in cases where the bond length sampling is needed. In these cases, the Cartesian displacement sampling can include the bond stretch degree of freedom to the fragment library.

Comparing the gas phase and in solution average values in Table 1, it can seen that the solvent effect is almost negligible for all bonds and angles, as expected. However, it is possible to identify a small stretching of approximately 0.01 Åin the C O bond in aqueous solution. This is an expected stretching caused by the Hydrogen bonds (HB) formed between the solute and solvent.[42,54] Therefore, a HB analysis was performed during the CBMC sampling and compared the rigid model of MOx in both conformations in aqueous solution. We used the geometrical and energetic criteria, as used before,[32] to identify the HB. These criteria are: the distance between the MOx oxygen and the water oxygen, $R(O_M \cdots O_W) \leq 3.25Å$, the angle between the the MOx oxygen and the oxygen-hydrogen covalent bond of water, $\theta(O_M \cdots O_W H) \leq 40^{\circ}$, and the binding energy, $E_{ij} \leq -0.01$kcal/mol. We selected $10^3$ statistically uncorrelated configurations from each simulation to perform the HB analysis and calculate the average number of water molecules forming HB with MOx $\langle N_{HB} \rangle$ and the average values of the geometric HB properties, such as $\langle R(O_M \cdots O_W) \rangle$ and $\langle \theta(O_M \cdots O_W H) \rangle$, and the HB binding energy, $\langle E_{ij} \rangle$. These values are shown in Table 2. As it can be seen, regardless the model of the MOx (rigid or flexible) the average and the standard deviation values are similar. Comparing the results obtained with the flexible model sampled with CBMC method and started with different MOx conformations, no difference was identified. However, for the MOx rigid model, a small difference was observed for the $\langle N_{HB} \rangle = 2.4 \pm 0.5$ HB at *syn* conformation and 2.8 ± 0.5 HB at *anti* conformation.

To analyze the sampling of the conformers we looked at the evolution of the C=C–C=O torsional angle during the simulations. As shown in Figure 3 the rotational energy profile presents two minima, one at 0° corresponding to the *syn* conformation and other at 180° corresponding to the *anti* conformation. The most stable is the *syn* conformation by approximately 1.3 kcal/mol and with a rotational barrier of approximately 10 kcal/mol. Therefore, with this energy difference between the *syn*- and *anti*-forms, it is expected a *syn:anti* population ratio of (91:9)%, meaning that 91% should be at *syn* conformation and 9% that *anti* conformation. A good sampling of the conformational population ratio is related to the accuracy of the average and standard deviation values of the torsional angle of the visited conformations, but also to the number of times that the visited conformations changes from one to another. The number of changes between the conformers is important because the equilibrium of the conformational populations ratio is only reached when the statistic of the conformational change is large enough to present a converged value of the population of each conformation. Sometimes the simulation can be trapped in one conformation due to the high-energy rotational barrier, which may be difficult to overcome. However, the ability of overcoming the energy barriers is fundamental to attain the ergodicity during the sampling. We compare the sampling of CBMC and MD simulations of the MOx in gas phase, showed in Figure 4. The plots in the top (Figure 4A) were initialized in the *anti* conformation and the plots in the bottom (b) started in the *syn* conformation.

As it can be seen, the CBMC simulations sample the same conformational space starting from different initial conditions (see Figure 4A,B at the left size), however, the MD simulations only samples around the initial conformation (see Figure 4A,B at right size) for a long time, approximately 400 ns (and ∼225 ns) for the simulation started with the *syn*-form (and *anti*-form). Doing a histogram over the CBMC torsional angle a

**TABLE 2** Analysis of the Hydrogen bonds between the MOx and the water molecules for rigid model of the solute and flexible model sampled with CBMC method using different initial condition: the *syn* and *anti* conformations

| Solute | $\langle N_{HB} \rangle$ | $\langle E_{ij} \rangle$ | $\langle R(O_M \cdots O_W) \rangle$ | $\langle \theta(O_M \cdots O_W H) \rangle$ |
|---|---|---|---|---|
| Rigid - *syn* | 2.4 ± 0.5 | −7.7 ± 1.7 | 2.75 ± 0.16 | 12 ± 7 |
| Rigid - *anti* | 2.8 ± 0.5 | −7.9 ± 1.8 | 2.76 ± 0.16 | 12 ± 7 |
| Flexible - *syn* start | 2.7 ± 0.5 | −8.0 ± 1.8 | 2.76 ± 0.16 | 12 ± 7 |
| Flexible - *anti* start | 2.7 ± 0.5 | −7.9 ± 1.7 | 2.76 ± 0.16 | 12 ± 7 |

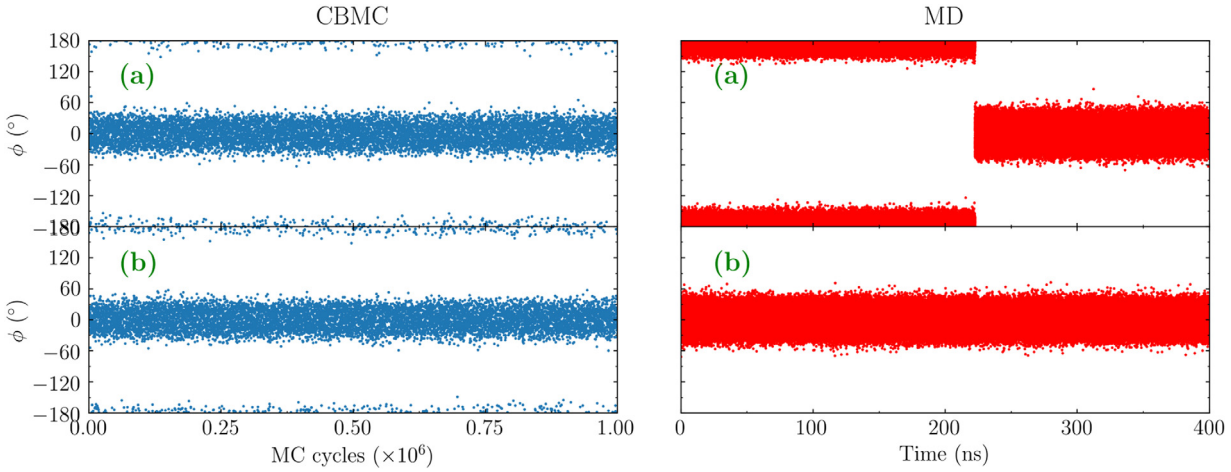


**FIGURE 4** Evolution of the C=C–C=O dihedral angle during the simulations of an isolated MOx molecule (in gas phase). In the top, the plots were labeled with (A) corresponding to the simulations started with MOx in the *anti* configuration (left with CBMC and right with MD) and in the bottom, the plots were labeled with (B) corresponding to simulations started in the *syn* conformation

bimodal distribution was found with one peak around the *syn* conformation, $\langle\phi_{C1C2C3O4}\rangle_{syn} = 0.3 \pm 19.8^{\circ}$ (and 0.1 ± 19.9°) for the simulation started with the *syn*-form (and *anti*-form), and another peak around the *anti* conformation, $\langle\phi_{C1C2C3O4}\rangle_{anti} = 179.8 \pm 9.5^{\circ}$ (and $179.7 \pm 9.7^{\circ}$) for the simulation started with the *syn*-form (and *anti*-form) (see, Table 1). Integrating each peak we obtained a *syn:anti* relative population of (95:5 ± 1)% (and (96:4 ± 1)%) for the simulation started with the *syn*-form (and *anti*-form). It means that around 95% of the conformations were sampled in the *syn*-form and 5% in the *anti*-form independently on the initial conformation. This result is in good agreement with the result predicted before (91% for the *syn* conformation and 9% for the *anti* conformation)[32] using the free energy difference, 1.34 kcal/mol, obtained with QM calculations.

The MD results for the $\phi_{C1C2C3O4}$ are not good, as the values depend on the initial conformation of the MOx. In Figure 4A at right side, the MOx starts at *anti* conformation, $\pm 180^{\circ}$, and stay there until approximately 225 ns. Then, it changes to the *syn* conformation, 0°, and stay there until the end of the simulation. Doing a histogram over these data a bimodal distribution was found with one peak around the *syn* conformation, $\langle\phi_{C1C2C3O4}\rangle_{syn} = 0.1 \pm 19.9^{\circ}$ and another peak around the *anti* conformation, $\langle\phi_{C1C2C3O4}\rangle_{anti} = 179.7 \pm 9.7^{\circ}$ (see values were showed in parenthesis in Table 1). Although integrating each peak we obtained a *syn:anti* relative population of 44:56 this relative population has no statistical meaning because only one conformational change was observed. In Figure 4B at right side, the MOx starts at *syn* conformation and stay there until until the end of the simulation. Doing a histogram over these data a monomial distribution was found with a peak around the *syn* conformation, $\langle\phi_{C1C2C3O4}\rangle_{syn} = 0.0 \pm 19.0^{\circ}$. In this simulation the *anti* conformation was not sampled, and 100% of the conformations were sampled in the *syn* conformation.

Figure 5 shows a comparison between the sampling of CBMC and MD simulations of the MOx in aqueous solution, like shown before in Figure 4 for the gas phase. Like in gas phase, the CBMC simulations sampled both conformers independently on the initial conformation of the

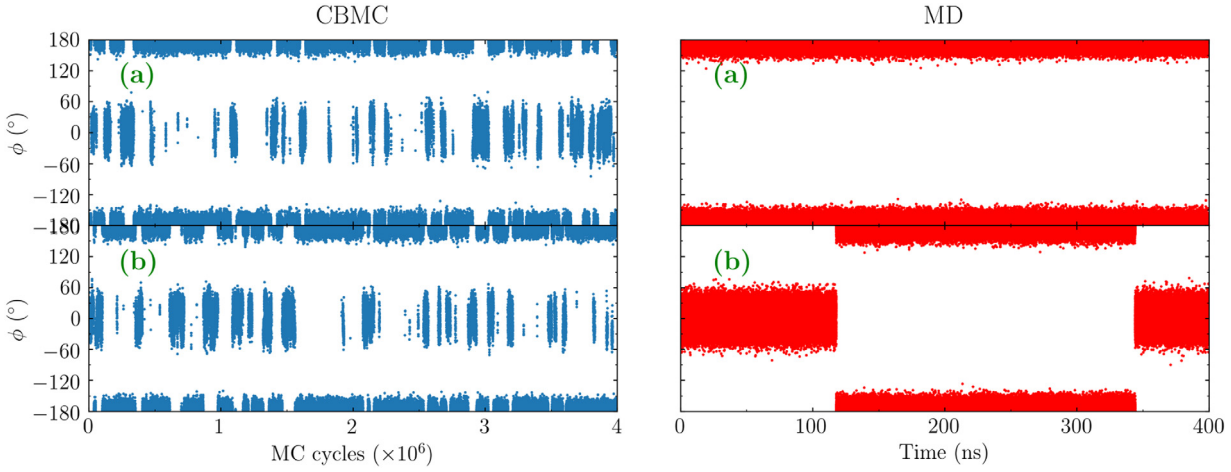


**FIGURE 5** Evolution of the C=C–C=O dihedral angle during the simulations of of MOx in aqueous solution. In the top, the plots were labeled with (A) corresponding to the simulations started with MOx in the *anti* configuration (left with CBMC and right with MD) and in the bottom, the plots were labeled with (B) corresponding to simulations started in the *syn* conformation. A, *syn* MOx, B, *anti* MOx, C, atomic labels

MOx. But now with a preference over the *anti* conformation. Doing a histogram over the CBMC torsional angle a bimodal distribution was found with one peak around the *syn* conformation, $\langle \phi_{C1C2C3O4} \rangle_{syn} = 0.2 \pm 25.3^{\circ}$ (and 2.0 ± 25.4°) for the simulation started with the *syn*-form (and *anti*-form), and another peak around the *anti* conformation, $\langle \phi_{C1C2C3O4} \rangle_{anti} = 179.7 \pm 10.1^{\circ}$ (and $179.7 \pm 10.2^{\circ}$) for the simulation started with the *syn*-form (and *anti*-form; see, Table 1). Integrating each peak we obtained a *syn:anti* relative population of (22:78 ± 7)% (and (27:73 ± 10)%) for the simulation started with the *syn*-form (and *anti*-form). Thus, around 25% of the conformations were sampled in the *syn*-form and 75% in the *anti*-form independently on the initial conformation. This result is in good agreement with the result predicted before[32] using the solvation thermodynamic cycle of the rigid *syn*- and *anti*-forms of the MOx in aqueous solution. It was found a inversion in the conformational stability caused by the change in the environment: the *syn* conformation more stable in gas phase and *anti* conformation in aqueous solution. They predict a free energy difference of −2.77 ± 1.09 kcal/mol that ensures 99% to 94% of the *anti* conformation in water. It is important to notice that our results has a qualitative agreement, but it presents a quantitative difference in the *syn:anti* conformational population ratio. This difference between the two work (previous[32] and ours) can be caused by their rigid model or by the difference in the solute–solvent interaction due to the water model (they used SPC and we used the SPC/E) and the small differences on the atomic charges for the MOx (they used QM calculated set of charges for each conformer and we used an average set of charge of both conformers, see details in subsection interatomic potential).

Comparing the CBMC conformational sampling of the MOx in gas phase and in aqueous solution (see left plots at Figures 4 and 5, respectively), it is possible to see that in gas phase there is an uniform distribution on the conformational changes during the entire simulation. However, in water this distribution is not uniform, with groups of successive MC cycles in each conformation. Analyzing the amount of successive MC cycles that belongs to each one of these groups, an average life time (or life cycle interval) of each conformation was obtained as approximately 44 600 (and ∼43 900) successive MC cycles in the *anti* conformation and approximately 12 600 (and ∼16 200) in the *syn* conformation for the simulation started with the *syn*-form (and *anti*-form). Thus, the MOx spends typically approximately 44 250 successive MC cycles in the *anti* conformation and approximately 14 400 in the *syn* conformation. Performing the same analysis in gas phase, it was obtained that the MOx spends typically approximately 110 successive MC cycles in the *anti* conformation and approximately 2300 in the *syn* conformation. Therefore, the amount of successive MC cycles was much larger with explicit water solvent, approximately 400 times more for the *anti* conformation and approximately 6 times more for the *syn* conformation, showing a larger stabilization of the *anti* conformation in aqueous solution. As analyzed in Table 2, the HB specific interaction formed between the MOx and water molecules are the same for both conformations. Then, this specific interaction can not be the origin of the *anti*-form stabilization in aqueous solution. Conversely, as discussed in subsection interatomic potential the dipole moment of the MOx in the *anti* conformation, 7.20 D, is larger than in the *syn* conformation, 5.22 D. Additionally, we calculated the average and the standard deviation values for the dipole moment of the MOx in gas phase and in aqueous solution. These values are 5.3 ± 0.4 D and 6.7 ± 0.8 D for the gas phase and aqueous solution, respectively, regardless the MOx initial conformation. Note that these values of dipole moment are consequences of the abundant population of *syn*-form in the gas phase and the *anti*-form in water. The larger MOx dipole in the *anti*-form than in *syn*-form ensures a larger the dipole-dipole solute–solvent interaction in favor of the *anti* conformation. Thus, this could be the origin of the strong stabilization of the *anti* conformation in aqueous solution.

The MD sampling of MOx in aqueous solution presents the same behavior of the gas phase simulations (see right plots at Figures 4 and 5). In both cases, it is strongly dependent on the initial conformation even for large solute–solvent simulations with 400 ns, and is unable to sample accordingly. Our results showed that the MD simulations can eventually overcome the rotational energy barrier, but the low number of conformational changes suggests that either enhanced sampling techniques or prohibitively long simulations would be needed to achieve a better sampling with this method. We performed two extra independent MD simulations of 150 ns each, to analyze this conformational change. It was obtained that for the MOx in aqueous solution the *syn:anti* conformational change is very rare in the MD simulations, as can be seen in Figures S2 and S3 of the Supporting Information. This limitation in the sampling is caused by the height of the rotational barrier, approximately 10 kcal/mol, relatively with the thermal energy, $kT \cong 0.6\text{kcal/mol}$. Thus, the MD sampling of the MOx is strongly dependent on the initial conformation even for large simulations with 150 ns up to 400 ns.

## 4 | CONCLUSIONS

In this work, we investigated the solvent effect on the *syn/anti* population ratio of Mesityl Oxide, using a new implementation of conformational bias Monte Carlo and molecular dynamics methods. For the MOx, we used the parameters of the OPLS-AA force field as used before[32] and additionally we re-parametrized some torsional angles involved in the *syn/anti* stability conformational to reproduce the free energy difference between the two conformers. Then, we obtained a rotational energy profile shown in Figure 3 with a rotational barrier of approximately 10 kcal $mol^{-1}$.

We used the same force field parameters for the MOx molecules and performed CBMC and MD simulations in the same thermodynamic conditions, both in gas phase and in aqueous solution, starting the simulations with different initial conditions: one with the MOx in the *syn*-form and another with the MOx in the *anti*-form. Comparing the results of these simulations, we showed that average values and standard deviations of intramolecular geometrical information such as bond lengths, angles, and torsional angles sampled in the CBMC and MD simulations are equivalent. However, the *syn/anti* population ratio was appropriately sampled only by the CBMC simulations. With the CBMC sampled configurations in gas phase, it was obtained 95% of the MOx conformations in the *syn*-form and 5% in the *anti*-form regardless of the initial conformation. Using

the same force field parameters for the MOx in aqueous solution, an inversion of the population was found, 25% in the *syn*-form and 75% in the *anti*-form. This result is in good agreement with the result predicted before (that in gas-phase the MOx exists dominantly in *syn*-form and in aqueous solution in *anti*-form)[32] using the free energy difference obtained with QM calculations in gas phase and the solvation thermodynamic cycles with FEP method to obtain the free energy difference in aqueous solution.

Comparing the gas phase and in-water CBMC sampling, it was observed that the MOx spends typically approximately 110 successive MC cycles in the *anti* conformation and approximately 2300 in the *syn* conformation in gas phase. However, it presents a much larger successive MC cycles with explicit water solvent, approximately 400 times more for the *anti* conformation, and approximately 6 times more for the *syn* conformation, showing a much larger stabilization of the *anti* conformation in aqueous solution. We conclude that this strong stabilization of the *anti* conformation in aqueous solution, does not come from the HB specific interaction formed between the MOx and water molecules because they are the same for both conformations. Instead, we believe it is a consequence of larger dipole-dipole solute–solvent interaction due to larger dipole moment of the MOx in the *anti* conformations (7.2 D) than in the *syn* conformation (5.2 D).

With the MD sampled configurations in gas phase and in aqueous solution, it was observed that the *syn*/*anti* conformational change is a very rare event. Thus, the MD sampling of the MOx is not appropriated because it is strongly dependent on the initial conformation even for large simulations with 150 ns up to 400 ns for the isolated solute and for solute–solvent systems.

Therefore, we conclude that our implementation leads to correct results and outperforms traditional MD when considering overcoming high energy barriers (∼10 kcal/mol).

This work clearly shows limitations of the MD sampling in the studies that involve large energy barrier such as *axial/equatorial* and *cis/trans* conformation stabilities. But it also shows that CBMC is an alternative method that can be used for this kind of studies at least for small and medium sized molecules.

## ACKNOWLEDGMENTS

This work was partially supported by CNPq, CAPES, FAPESP, INCT-FCx, NAP-FCx(USP), and BioMol (Brazil). Additionally, HMC acknowledges the PhD fellowship from CNPq, and SC and KC the research fellowships from CNPq.

## REFERENCES

1. C. Reichardt, *Solvents and Solvent Effects in Organic Chemistry*, 4th ed., Wiley-VCH, Weinheim, Germany 2011.
2. C. Dugave, L. Demange, Chem. Rev. 2003, 103, 2475.
3. K. Tanabe, Spectrochim. Acta A 1972, 28A, 407.
4. K. B. Wiberg, T. A. Keith, M. J. Frisch, M. Murcko, J. Phys. Chem. 1995, 99, 9072.
5. L. Tauscher, S. Ghisla, P. Hemmerich, Helv. Chim. Acta 1973, 56, 630.
6. J. D. Engel, P. H. V. Hippel, Biochemistry 1974, 13, 4143.
7. M. L. DeRider, S. J. Wilkens, M. J. Waddell, L. E. Bretscher, F. Weinhold, R. T. Raines, J. L. Markley, J. Am. Chem. Soc. 2002, 124, 2497.
8. H. Katagiri, T. Hattori, N. Morohashi, N. Iki, S. Miyano, J. Org. Chem. 2007, 72, 8327.
9. S. Pedersoli, C. F. Tormena, R. Rittner, J. Mol. Struct. 2008, 875, 235.
10. G. Alagona, C. Ghio, J. Phys. Chem. A 2006, 110, 647.
11. P. I. Nagy, Molecules 2013, 18, 8063.
12. T. A. Mohamed, A. E. Hassan, I. A. Shaaban, A. M. Abuelela, W. M. Zoghaib, J. Mol. Struct. 2017, 1130, 434.
13. M. P. Allen, D. J. Tildesley, *Computer Simulation of Liquids*, Oxford University Press, Oxford 1989.
14. D. Frenkel, B. Smit, *Understanding Molecular Simulation*, 2nd ed., Academic Press, San Diego 2002.
15. Y. Sugita, Y. Okamoto, Chem. Phys. Lett. 1999, 314, 141.
16. D. Hamelberg, J. Mongan, J. A. McCammon, J. Chem. Phys. 2004, 120, 11919.
17. B. J. Berne, J. E. Straub, Curr. Opin. Struct. Biol. 1997, 7, 181.
18. W. L. Jorgensen, J. Tirado-Rives, J. Phys. Chem. 1996, 100, 14508.
19. J. P. Ulmschneider, M. B. Ulmschneider, A. D. Nola, J. Phys. Chem. B 2006, 110, 16733.
20. M. Z. Hernandes, R. Longo, K. Coutinho, S. Canuto, Phys. Chem. Chem. Phys. 2004, 6, 2088.
21. L. B. Oliveira, T. L. Fonseca, K. Coutinho, S. Canuto, Chem. Phys. Lett. 2011, 514, 251.
22. N. A. Murugan, H. Ågren, J. Phys. Chem. A 2009, 113, 2572.
23. J. I. Siepmann, D. Frenkel, Mol. Phys. 1992, 75, 59.
24. M. G. Martin, J. I. Siepmann, J. Phys. Chem. B 1999, 103, 4508.
25. J. K. Shah, E. J. Maginn, J. Chem. Phys. 2011, 135, 134121.
26. A. Sepehri, T. D. Loeffler, B. Chen, J. Chem. Theory Comput. 2017, 13, 1577.
27. A. Sepehri, T. D. Loeffler, B. Chen, J. Chem. Theory Comput. 2017, 13, 4043.
28. M. D. Macedonia, E. J. Maginn, Mol. Phys. 1999, 96, 1375.
29. F. H. Stross, J. M. Monger, H. V. Finch, J. Am. Chem. Soc. 1947, 69, 1627.
30. H. F. Gray, Jr, R. S. Rasmussen, D. D. Tunnicliff, J. Am. Chem. Soc. 1947, 69, 1630.
31. E. M. Kosower, J. Am. Chem. Soc. 1958, 80, 3261.
32. M. V. A. Damasceno, B. J. C. Cabral, K. Coutinho, Theor. Chem. Acc. 2012, 131, 1214.
33. K. Coutinho, S. Canuto, *Dice: A Monte Carlo Program for Molecular Liquid Simulation, University of São Paulo, V1.0*, São Paulo, Brazil 1993.
34. K. Coutinho, S. Canuto, *Dice: A Monte Carlo Program for Molecular Liquid Simulation, University of São Paulo, V2.9*, São Paulo, Brazil 2013.
35. K. Coutinho, S. Canuto, J. Mol. Struct. THEOCHEM 1993, 287, 99.
36. K. Coutinho, S. Canuto, M. C. Zerner, Int. J. Quantum Chem. 1997, 65, 885.

37. J. C. Owicki, *Optimization of Sampling Algorithms in Monte Carlo Calculations on Fluids*, American Chemical Society, Washington DC, USA 1978, Ch. 14, pp. 159–171.
38. B. Bigot, W. L. Jorgensen, J. Chem. Phys. 1981, 75, 1944.
39. R. W. Zwanzig, J. Chem. Phys. 1954, 22, 1420.
40. W. Jorgensen, J. Buckner, S. Boudon, J. Tirado-Rives, J. Chem. Phys. 1988, 89, 3742.
41. J. K. Shah, E. Marin-Rimoldi, R. G. Mullen, B. P. Keene, S. Khan, A. S. Paluch, N. Rai, L. L. Romanielo, T. W. Rosch, B. Yoo, E. J. Maginn, J. Comput. Chem. 2017, 38, 1727.
42. K. Coutinho, N. Saavedra, S. Canuto, J. Mol. Struct. THEOCHEM 1999, 466, 69.
43. W. L. Jorgensen, D. S. Maxwell, J. Tirado-Rives, J. Am. Chem. Soc. 1996, 118, 11225.
44. H. J. C. Berendsen, J. R. Grigera, T. P. Straatsma, J. Phys. Chem. 1987, 91, 6269.
45. H. Georg, K. Coutinho, S. Canuto, Chem. Phys. Lett. 2006, 429, 119.
46. C. Breneman, K. Wiberg, J. Comput. Chem. 1990, 11, 361.
47. C. Moller, M. Plesset, Phys. Rev. 1934, 46, 618.
48. T. Dunning, Jr, J. Chem. Phys. 1989, 90, 1007.
49. H. M. Cezar, S. Canuto, K. Coutinho, *Dice: A Monte Carlo Program for Molecular Liquid Simulation, University of São Paulo, V. 3.0*, São Paulo, Brazil 2017.
50. S. Pronk, S. Páll, R. Schulz, P. Larsson, P. Bjelkmar, R. Apostolov, M. R. Shirts, J. C. Smith, P. M. Kasson, D. van der Spoel, B. Hess, E. Lindahl, Bioinformatics 2013, 29, 845.
51. G. Bussi, D. Donadio, M. Parrinello, J. Chem. Phys. 2007, 126, 014101.
52. H. J. C. Berendsen, J. P. M. Postma, W. F. van Gunsteren, A. DiNola, J. R. Haak, J. Chem. Phys. 1984, 81, 3684.
53. B. Hess, H. Bekker, H. J. C. Berendsen, J. G. E. M. Fraaije, J. Comput. Chem. 1997, 18, 1463.
54. H. Wang, L. Wang, S. Shen, W. Zhang, M. Li, L. Du, X. Zheng, D. L. Phillips, J. Chem. Phys. 2012, 136, 124509.


## SUPPORTING INFORMATION

Additional supporting information may be found online in the Supporting Information section at the end of the article.

**How to cite this article:** Cezar HM, Canuto S, Coutinho K. Solvent effect on the *syn/anti* conformational stability: A comparison between conformational bias Monte Carlo and molecular dynamics methods. *Int J Quantum Chem*. 2019;119:e25688. https://doi.org/10.1002/qua.25688

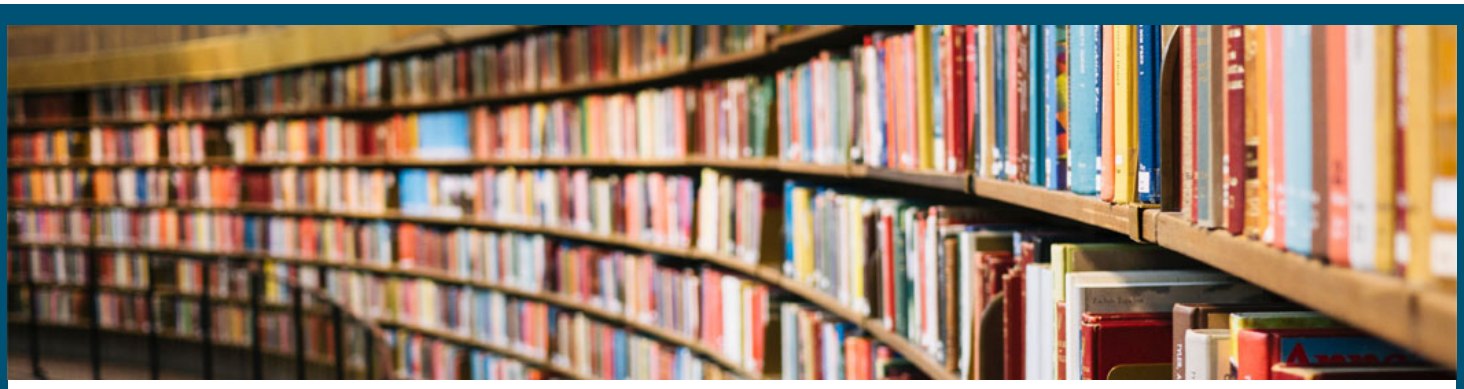

# TOP DOWNLOADED PAPER 2018-2019

CONGRATULATIONS TO

# Kaline Coutinho

whose paper has been recognized as
one of the most read in

**International Journal of Quantum Chemistry**

WILEY